Statistical properties of effective elastic moduli of random cubic polycrystals

Ningyue Sheng, Shahram Khazaie, Mathilde Chevreuil, Sylvain Fréour

Mechanics & Industry **24**, 33 (2023)

https://doi.org/10.1051/meca/2023030

Mechanics & Industry

Available online at:
www.mechanics-industry.org

History of matter: from its raw state to its end of life
Prof. Amine Ammar (Guest Editor)

REGULAR ARTICLE

OPEN ACCESS

Statistical properties of effective elastic moduli of random cubic polycrystals

Ningyue Sheng*, Shahram Khazaie, Mathilde Chevreuil, and Sylvain Fréour

Nantes Université, Ecole Centrale Nantes, CNRS, GeM, UMR 6183, 44000 Nantes, France

Received: 23 December 2022 / Accepted: 4 August 2023

Abstract. The homogenized elastic properties of polycrystals depend on the grain morphology and crystallographic orientations. For simplification purposes, the orientations of the grains are usually considered three independent Euler angles. However, experimental investigations reveal spatial correlations in these angles. The Karhunen–Loève expansion is used to generate random fields of Euler angles having exponential kernel functions with varying correlation lengths. The effective elastic moduli for numerically generated statistically equiaxed cubic polycrystals are estimated via the classical Eshelby–Kröner Self-Consistent homogenization model. The influence of the correlation lengths of the orientations' random fields on the statistical properties of the effective elastic moduli has been investigated. Our results show that spatially correlated Euler angles could increase the variability of the homogenized elastic properties compared to the ones having uncorrelated Euler angles. Nevertheless, using independent random variables for Euler angles remains valid when correlation lengths are close to the average grain size.

Keywords: Polycrystals / random fields / effective elastic moduli / Karhonen–Loève expansion

1 Introduction

Polycrystalline materials are widely used and play a key role in many engineering applications for which effective mechanical properties are often of great concern. The former are discrete crystallites or grains with different morphological and crystallographic characteristics. Numerous investigations have focused on how these characteristics ultimately influence the effective mechanical properties at the macroscopic scale.

In most previous numerical works, the crystallographic orientations of the grains in polycrystals are represented by introducing the randomness on a triplet of Euler angles $(\Theta_1, \Theta, \Theta_2)$, that are usually considered as statistically independent random variables [1–3]. This assumption simplifies the numerical generation process of the Euler angles in the polycrystalline samples. However, in real polycrystals, the crystallographic orientations may be spatially correlated due to the grain nucleation and growth mechanisms. For instance, grains with similar orientations tend to form low-energy boundaries between them, facilitating cooperative growth along specific directions. This grain-to-grain interaction leads to spatially correlated orientations within the polycrystal. Besides, experimental investigations also report the spatial correlation of the grain orientations [4–6]. In addition, in order to get the aimed performance, some special metalworking processes like extrusion and drawing are widely used when manufacturing polycrystalline materials. These processes may induce a strong crystallographic and morphological texture, referring to a particular spatial arrangement of grains with strongly correlated crystallographic orientations in the polycrystal. A common way to represent these spatial correlations is by constructing random fields of the Euler angles [6].

The impact of the parameters of the Euler angles' random fields on the effective mechanical properties has not been investigated yet. In the present study, we consider an exponential kernel function, frequently used in the literature, and two different correlation lengths to cover a range of the size of inhomogeneities in the numerically simulated Euler angles' random fields.

In this paper, the numerical simulation of the random fields of orientations, along with the polycrystal models, will be introduced in Sections 2.1 and 2.2. The classical Eshelby–Kröner Self-Consistent model explained in Section 2.3, is used in the present work to estimate the effective elastic moduli of the simulated polycrystals. The influence of the correlation length of the random fields of Euler angles on the statistical properties of the effective elastic moduli is presented and discussed in Section 3.

* e-mail: shahram.khazaie@univ-nantes.fr

Table 1. Basic information of synthetic polycrystal sample sets.

Name	Poly-1	Poly-2	Poly-3	Poly-4	Poly-5	Poly-6
N_g	50	100	500	1000	5000	10000
$\bar{D}_{\mathrm{eq}}$ [μm]	305.4	240.0	139.3	110.6	64.6	51.3
$\sigma_{D_{\mathrm{eq}}}$ [μm]	100.3	82.0	48.8	38.7	22.7	18.0
$\delta_{D_{\mathrm{eq}}}$ [–]	0.33	0.34	0.35	0.35	0.35	0.35

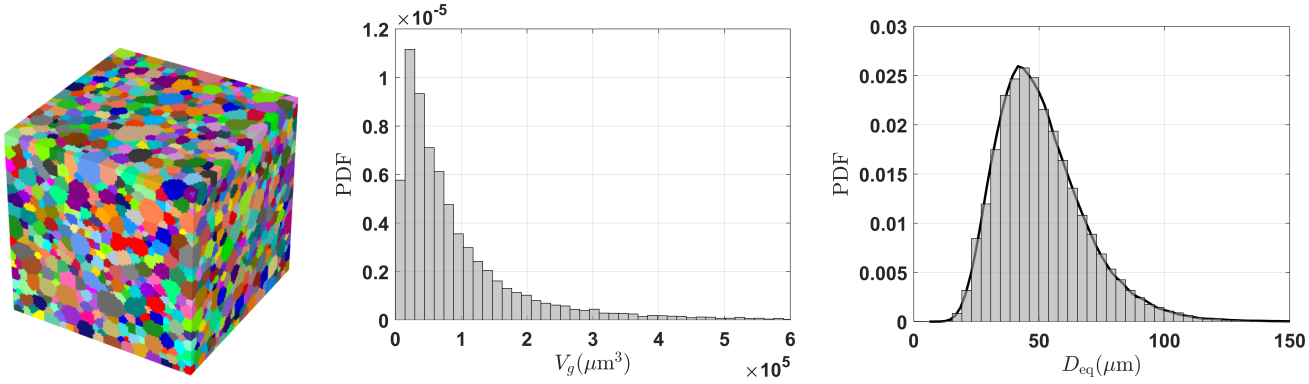

Fig. 1. A realization of a polycrystal having 10000 grains (left), the PDF of its grain volumes (middle), and the PDF of its grain sizes D_{eq} (histogram, right) compared with the target one (black solid line, right).

2 Numerical model construction and computational framework

2.1 Numerical cubic polycrystal model

Using the open-source software NEPER [7], multiple synthetic polycrystals containing different numbers of grains are generated. These grains exhibit a statistically equiaxed morphology, with statistically equal dimensions in all three spatial directions (x, y, and z), without any prominent elongation or flattening on the grain shapes. Moreover, the values of the probability density function (PDF) of the aspect ratio should be peaked around 1 and should have a small coefficient of variation. Each polycrystal is a cube of side 1000 μm. The number of grains N_g, as well as the first- and second-order statistics of the grain size, *e.g.*, the mean ($\bar{D}_{\mathrm{eq}}$), the standard deviation ($\sigma_{D_{\mathrm{eq}}}$), and the coefficient of variation ($\delta_{D_{\mathrm{eq}}}$) of the grain equivalent diameters D_{eq} of different sample sets, are given in Table 1. It should be noted that the equivalent diameter of each grain is defined as the diameter of a sphere having the same volume as the grain. Besides, the grain sizes follow a lognormal distribution, as reported in experimental investigations [8–10]. The values of $\delta_{D_{\mathrm{eq}}}$ are set around 0.35 for all sample sets, considerably smaller than those observed in real polycrystalline samples, which can exceed 1 [8]. For each sample set, 200 realizations are generated (1200 samples in total). It should be mentioned that the size and the centroid location of the grains in the polycrystals vary between different realizations. Raster tessellation is used to generate microstructures in order to get closer to the morphological characteristics of the real grains [11,12]. Figure 1 (left) shows one of the realizations having 10000 grains, in which the grains are distinguished with different colors. The histogram of the volumes of the grains that also follows a lognormal distribution is depicted in the same figure (middle). Moreover, the histogram of D_{eq} for this realization closely matches the target PDF (black solid line), shown in Figure 1 (right).

Table 2. Parameters of numerically simulated Euler angles.

Name	Kernel function	Correlation length
Uncorrelated	/	/
C-S	Exponential	$l_X^s = \bar{D}_{\mathrm{eq}}$
C-L	Exponential	$l_X^l = 10\bar{D}_{\mathrm{eq}}$

2.2 Random fields of Euler angles

Based on the numerically generated polycrystal models, we subsequently aimed to simulate the crystallographic orientations of the grains. For comparison purposes, these Euler angles are considered either uncorrelated (Θ_1^{uc}, Θ^{uc}, Θ_2^{uc}), or spatially correlated (Θ_1, Θ, Θ_2). For the case **Uncorrelated** in Table 2, the Euler angles are assumed to be statistically independent random variables, yielding uniform random rotations and a textureless random polycrystal. More specifically, Θ_1^{uc} and Θ_2^{uc} are uniformly distributed random variables between [0, 2π], while Θ^{uc} is a random variable following Gilbert's sine distribution in [0, π] to achieve statistical isotropy in the polycrystal. These random Euler angles can be easily simulated as follows [13]:

$$\Theta_1^{uc} = 2\pi X_1, \quad \Theta^{uc} = \arccos(-1 + 2X_2), \quad \Theta_2^{uc} = 2\pi X_3, \tag{1}$$

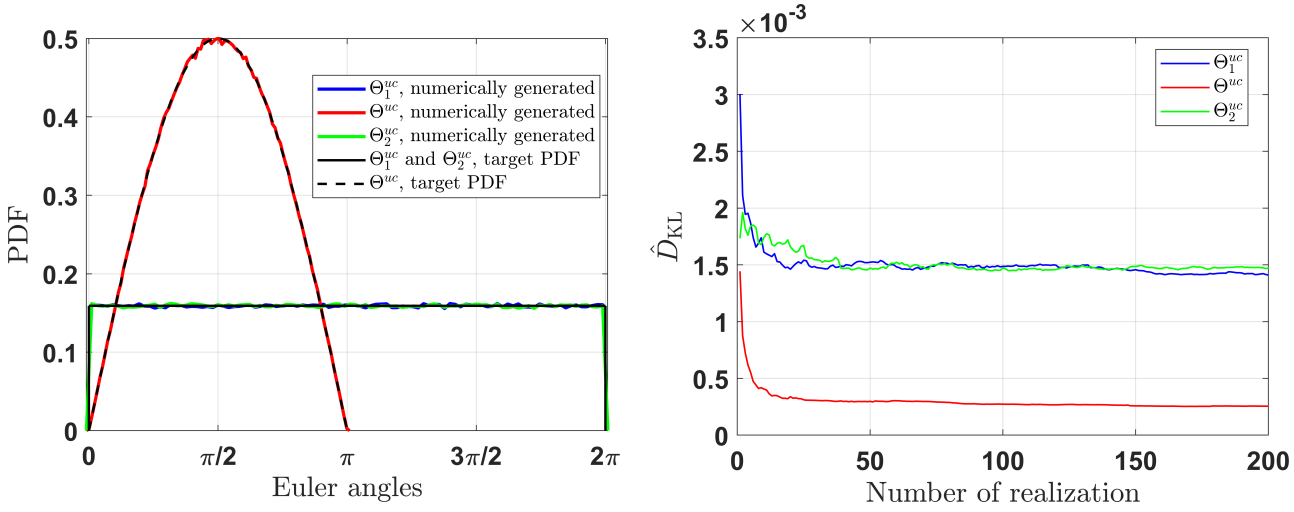

Fig. 2. PDFs of numerically simulated and target uncorrelated Euler angles with statistical isotropy in 200 realizations of **Poly-6** model (left), and their measured normalized relative entropy, as a function of the number of realizations (right).

in which $X_i \in \mathrm{U}(0,1)$ $(i \in \{1,2,3\})$ are three independent uniform random variables. The PDFs of numerically simulated uncorrelated Euler angles, based on 200 realizations of **Poly-6** model, are presented in Figure 2, and compared with the target distributions. The relative entropy D_{KL} (Kullback–Leibler divergence) [14,15] has been used as the measure to evaluate the distance between the PDFs of the numerically generated Euler angles $P_1(x)$ and the target ones $P_2(x)$. The former is defined as:

$$D_{\mathrm{KL}}\left(P_1 \parallel P_2\right) = \int_{-\infty}^{+\infty} P_1(x) \log\left(\frac{P_1(x)}{P_2(x)}\right) \mathrm{d}x. \quad (2)$$

Considering the normalization through a nonlinear transformation $\hat{D}_{\mathrm{KL}} = 1 - \exp\left(-D_{\mathrm{KL}}\right)$, the plot of the normalized relative entropy $\hat{D}_{\mathrm{KL}}$, as a function of the number of realizations, is shown in Figure 2 (right). The small values of relative entropy after 200 realizations indicate that the PDFs of simulated Euler angles are close to the target ones.

The spatially correlated crystallographic orientations of the grains can be represented by constructing correlated non-Gaussian random fields of Euler angles. We first generated a vector containing three Gaussian random fields $\mathbf{Z}(\mathbf{p}) = [Z_1(\mathbf{p}), Z_2(\mathbf{p}), Z_3(\mathbf{p})]$, where $\mathbf{p}$ is the spatial centroid position of each grain, having the given target auto-covariance functions (ACFs) via the Karhunen–Loève expansion [16,17]. The target ACFs of Θ_1, Θ and Θ_2 are supposed to be isotropic so that they only depend on the distance between the centroid positions of the grains. In this paper, we consider an exponential ACF based on [18]:

$$C_{XX}\left(\mathbf{p}_m, \mathbf{p}_n\right) = \exp\left(-2\frac{\|\mathbf{p}_m - \mathbf{p}_n\|}{l_X}\right), \quad (3)$$

in which $\mathbf{p}_m$ and $\mathbf{p}_n$ $(m,n \in \{1,...,N_g\})$ are the centroid positions of any two grains in the polycrystal and l_X $(X \in (\Theta_1, \Theta, \Theta_2))$ is the correlation length of the random field. In our numerical study, the case **C-S**, with a relatively short correlation length l_X^s and the case **C-L**, with a relatively long correlation length l_X^l are considered as shown in Table 2. The correlation lengths l_X^s and l_X^l were defined as a multiple of the mathematical expectation of the grain equivalent diameter $\bar{D}_{\mathrm{eq}}$ in each realization as:

$$\begin{aligned} l_X^s &= \left(l_{\Theta_1}^s, l_{\Theta}^s, l_{\Theta_2}^s\right) = \left(\bar{D}_{\mathrm{eq}}, \bar{D}_{\mathrm{eq}}, \bar{D}_{\mathrm{eq}}\right), \\ l_X^l &= \left(l_{\Theta_1}^l, l_{\Theta}^l, l_{\Theta_2}^l\right) = 10\left(\bar{D}_{\mathrm{eq}}, \bar{D}_{\mathrm{eq}}, \bar{D}_{\mathrm{eq}}\right). \end{aligned} \quad (4)$$

It should be noted that the **Uncorrelated** case may be imagined as the scenario where the ratio between the correlation length and average grain diameter is 1/2. The KLE is a series expansion method based on the spectral decomposition of the ACF of the random field. In practice, the KLE can be approximated by truncating at a finite number of terms in order to numerically simulate the Gaussian random fields $Z_i(\mathbf{p})$:

$$Z_i(\mathbf{p}) \approx \sum_{k=1}^{N_g} \sqrt{\lambda_k^i}\gamma_k^i \psi_k^i(\mathbf{p}), \quad i \in \{1,2,3\}, \quad (5)$$

where $\left\{\lambda_k^i, \psi_k^i\right\}$ are the eigenvalues with their corresponding eigenfunctions of the target ACF, and γ_k^i is a vector of independent standard Gaussian random variables. The memoryless transforms of the standard Gaussian processes are used to simulate non-Gaussian processes [19,20]. Based on the known marginal cumulative distribution functions (CDFs), the simulation of the target non-Gaussian random fields could be performed by the so-called non-Gaussian translation processes [21]:

$$\tilde{Z}_i(\mathbf{p}) = F_{\tilde{Z}_i}^{-1}\left(\mathbf{\Phi}\left(Z_i(\mathbf{p})\right)\right), \quad i \in \{1,2,3\}, \quad (6)$$

$$\mathbf{t}=\begin{bmatrix}-\cos(\Theta)\sin(\Theta_1)\sin(\Theta_2)+\cos(\Theta_1)\cos(\Theta_2) & -\cos(\Theta)\cos(\Theta_2)\sin(\Theta_1)-\cos(\Theta_1)\sin(\Theta_2) & \sin(\Theta_1)\sin(\Theta)\\ \cos(\Theta)\cos(\Theta_1)\sin(\Theta_2)+\cos(\Theta_2)\sin(\Theta_1) & \cos(\Theta)\cos(\Theta_1)\cos(\Theta_2)-\sin(\Theta_1)\sin(\Theta_2) & -\cos(\Theta_1)\sin(\Theta)\\ \sin(\Theta_2)\sin(\Theta) & \cos(\Theta_2)\sin(\Theta) & \cos(\Theta)\end{bmatrix}. \tag{9}$$

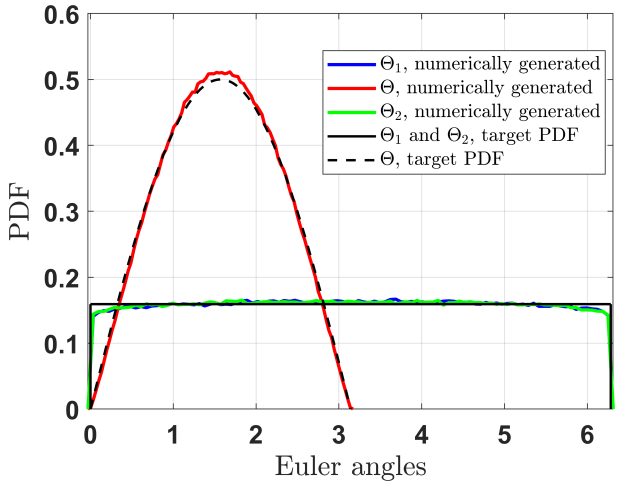

Fig. 3. The non-Gaussian random fields of Euler angles $(\Theta_1, \Theta, \Theta_2)$ having **C-S** parameters compared with the target PDFs in 200 realizations for the model **Poly-6**.

in which $F_{\tilde{Z}_i}(x)=\int_{-\infty}^{x} p_{\tilde{Z}_i}(y)\mathrm{d}y$ is the CDF of $\tilde{Z}_i$ with target PDF $p_{\tilde{Z}_i}$, and $\mathbf{\Phi}(\cdot)$ is the target CDF of the standard Gaussian distribution. We subsequently used this method to simulate the correlated Euler angles with different parameters for each grain in each realization of different polycrystal models listed in Table 1. The PDFs of the non-Gaussian random fields of the Euler angles $(\Theta_1, \Theta, \Theta_2)=(\tilde{Z}_1, \tilde{Z}_2, \tilde{Z}_3)$ with the parameters **C-S** are shown in Figure 3, for 200 realizations of **Poly-6**. According to this figure, the PDFs of the numerically simulated correlated Euler angles appropriately match the target PDFs. Furthermore, it is expected that augmenting the number of realizations will lead to a more accurate convergence with the target PDFs.

Statistical convergence has been investigated on the numerically generated Euler angles by calculating the relative errors of the relevant statistical quantities over 200 realizations for each model shown in Figure 4. Here, the relative errors were defined as the normalized gradient of the cumulative mean and the cumulative coefficient of variation. The convergence criterion was set as the relative error being less than 2%. Figure 4 illustrates the statistical convergence of the generated Euler angles with the parameters **C-L** for **Poly-1** up to 200 realizations. The results highlight a good convergence of the first- and second-order statistics of the random fields using 200 realizations. For all other cases, similar observations have been made.

2.3 Computational framework for effective elastic moduli

The classical Eshelby–Kröner Self-Consistent (SC) model will be subsequently used to estimate the effective elasticity tensor of polycrystals. Eshelby [22] has shown that according to the equivalent inclusion method, under the assumption of linear elasticity and small deformation, in an unbounded homogeneous isotropic medium submitted to an applied uniform macroscopic strain ϵ_{kl} in the far field, the strain in the embedded ellipsoid is also uniform with $\epsilon_{ij}^{\mathrm{inc}}=A_{ijkl}\epsilon_{kl}$, where A_{ijkl} is the so-called localization tensor, and $\epsilon_{ij}^{\mathrm{inc}}$ and ϵ_{kl} are the uniform strains inside the ellipsoid and in the far field, respectively. Based on Eshelby's theory, Kröner [23] introduced the SC method to estimate the elastic moduli of polycrystals from single crystal elastic constants of cubic symmetry. Lubarda [24] proposed the method to estimate the effective elastic moduli for the isotropic polycrystals with cubic crystals, which is an extension of the SC method. He showed that if a single cubic crystal with a spherical shape is surrounded by an effective isotropic polycrystalline aggregate, the concentration tensor has the form:

$$A_{ijkl}=I_{ijkl}+a\left(\delta_{ij}\delta_{kl}+2I_{ijkl}-5T_{ijkl}\right), \tag{7}$$

in which $I_{ijkl}=\frac{1}{2}\left(\delta_{ik}\delta_{jl}+\delta_{il}\delta_{jk}\right)$ is the fourth-order identity tensor, δ_{ij} $(i,j\in\{1,2,3\})$ is the Kronecker delta, being 1 when $i=j$, and 0 otherwise. The explicit formula of a writes:

$$\begin{aligned}a=&\frac{(c_{11}+2c_{12}+6b)(c_{11}-c_{12}-2b)}{3\left[8b^2+9c_{11}b+(c_{11}-c_{12})(c_{11}+2c_{12})\right]},\\ &8b^3+(5c_{11}+4c_{12})\,b^2-c_{44}\,(7c_{11}-4c_{12})\,b\\ &-c_{44}\,(c_{11}-c_{12})\,(c_{11}+2c_{12})=0,\end{aligned} \tag{8}$$

where c_{IJ} $(IJ\in\{11,12,44\})$ are the components of elastic constants in the crystallite's local reference, and b is the positive real root of the given cubic polynomial [23].

In equation (7), T_{ijkl} is the rotation tensor and can be expressed in the form $T_{ijkl}=\sum_{m=1}^{3} t_{im}t_{jm}t_{km}t_{lm}$ $(\{i,j,k,l\}\in\{1,2,3\})$. The corresponding rotation matrix $\mathbf{t}$ is defined as [13]:

see equation 9 above

Based on the theory proposed by Eshelby and equation (7), Lubarda [24] derived the elastic modulus of n^{th} crystallite with spherical geometry as:

$$\begin{aligned}C_{ijkl}^{\mathrm{sc},n}=C_{ijkl}^{n}+a\Big[&(c_{11}-c_{12})\delta_{ij}\delta_{kl}+4c_{44}I_{ijkl}\\ &-\left[3\,(c_{11}-c_{12})+4c_{44}\right]T_{ijkl}^{n}\Big],\end{aligned} \tag{10}$$

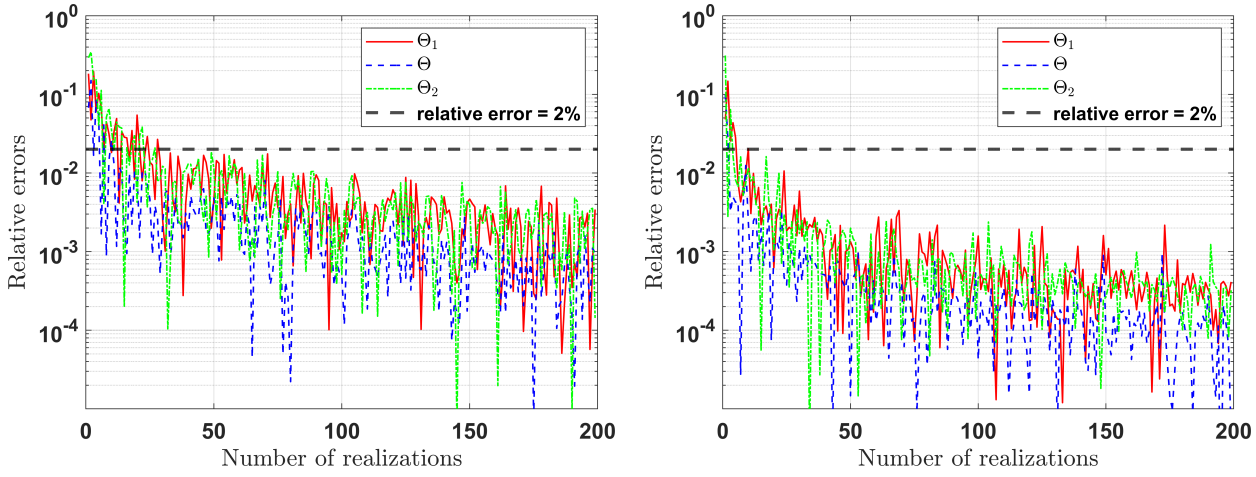

Fig. 4. Relative errors (normalized gradient) of the cumulative mean (left), and of the cumulative coefficient of variation (right) of the generated Euler angles with parameters **C-L** for **Poly-1** over 200 realizations.

Table 3. Single crystal elastic constants and their anisotropy factors of eleven cubic materials [26].

Name	Al	Cr	Ta	Pt	Fe	Ni	Au	Co	Cu	K	Li
c_{11}	108	348	264	347	230	247	191	242	169	3.71	13.4
c_{12}	62	67	158	251	135	153	162	160	122	3.15	11.3
c_{44}	28.3	100	82.6	76.5	117	122	42.2	128	75.3	1.88	9.6
A	0.23	0.29	0.56	0.59	1.46	1.60	1.91	2.12	2.20	5.71	8.14

where the elasticity tensor C^n_{ijkl} of n^{th} cubic crystallite in the laboratory reference frame reads:

$$C^n_{ijkl} = c_{12}\left(\delta_{ij}\delta_{kl}\right) + c_{44}\left(\delta_{ik}\delta_{jl} + \delta_{il}\delta_{jk}\right) + \nu T^n_{ijkl}, \quad (11)$$

in which ν is the anisotropy coefficient of the single crystal, defined as $\nu = c_{11} - c_{12} - 2c_{44}$. The effective elasticity tensor of each polycrystal with total volume V and N_g grains can then be calculated using the volume average:

$$\langle C^{\text{eff}}_{ijkl}\rangle = \frac{1}{V}\int_\Omega C^{\text{sc},n}_{ijkl}(\mathbf{x})\mathrm{d}\mathbf{x} = \frac{1}{V}\sum_{n=1}^{N_g} C^{\text{sc},n}_{ijkl}V_n, \quad (12)$$

where the integration domain Ω is the whole volume of the polycrystal, $V = \int_\Omega \mathrm{d}\mathbf{x}$, and V_n is the volume of n^{th} grain in polycrystal.

3 Results and discussion

The statistical properties of effective elastic moduli have been investigated on different cubic materials, listed in Table 3. The normalized single crystal anisotropy factor is defined as $A = |1 - A_Z|$, where $A_Z = 2c_{44}/(c_{11} - c_{12})$ is the so-called Zener anisotropy factor [25]. For the particular case of isotropy, A_Z equals 1 and thus A vanishes. Based on the values of A presented in Table 3, aluminum (Al) has the lowest normalized anisotropy factor, while lithium (Li) has the largest one.

The effective elastic moduli of the synthetic polycrystals are estimated using the aforementioned SC approach. Figure 5 presents the PDFs of the effective elasticity tensor component C^{eff}_{11}. These PDFs are estimated for iron (Fe) using 200 realizations of each polycrystal sample set **Poly-2**, **Poly-4**, and **Poly-6**, considering the Euler angles as uncorrelated (case **Uncorrelated**) and correlated with a relatively long correlation (case **C-L**). It clearly shows that increasing the number of grains (N_g) decreases the variance of the corresponding distributions of the effective elastic moduli, regardless of the microstructural details of the random polycrystals.

The standard deviations of the effective elastic moduli are subsequently calculated for better investigating the influence of correlated and uncorrelated Euler angles for the case **Uncorrelated**, **C-S** and **C-L** on the statistical properties:

$$\bar{Y} = \frac{1}{N_r}\sum_{i=1}^{N_r} y_i, \quad \sigma_Y = \sqrt{\frac{1}{N_r - 1}\sum_{i=1}^{N_r}(y_i - \bar{Y})^2}, \quad (13)$$

wherein N_r is the number of the realizations of each polycrystal model, being $N_r = 200$ in this study. Y is the quantity of interest, and $\bar{Y}$ and σ_Y are its expectation and standard deviation, respectively. Here, the random variable of interest is the component C^{eff}_{11} of the effective macroscopic elasticity tensor.

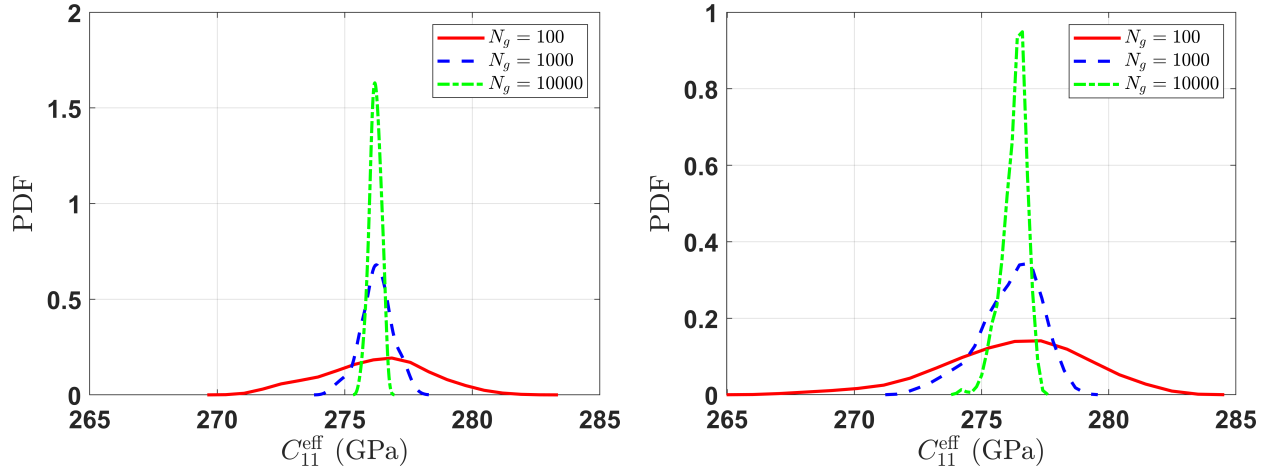

Fig. 5. PDFs of the component C_{11}^{eff} of effective elasticity tensor of iron (Fe) using 200 realizations of **Poly-2** (100 grains per realization), **Poly-4** (1000 grains per realization) and **Poly-6** (10000 grains per realization) with **Uncorrelated** (left), and **C-L** (right) types of Euler angles.

Following [3], in order to obtain a master curve for all materials, the standard deviations of C_{11}^{eff} ($\sigma_{C_{11}^{\text{eff}}}$) are normalized by the absolute value of the anisotropy coefficient of the SC approach ν_{sc}, which is defined as $\nu_{\text{sc}} = \nu(1-3a) - 10a\, c_{44}$, for all the cases in our study. It is obvious that $\sigma_{C_{11}^{\text{eff}}}$ is linearly proportional to ν_{sc}. As shown in Figure 6, regardless of the parameters of Euler angles, the normalized standard deviations of C_{11}^{eff} for all materials with different N_g are dominated by three main linear curves in a log-scale. Furthermore, an inverse relationship was observed between the normalized $\sigma_{C_{11}^{\text{eff}}}$ and N_g. The main curves, denoted as f_1, f_2 and f_3 in the legends of Figure 6, can be expressed as a function linking $\sigma_{C_{11}^{\text{eff}}}$ to N_g, each with different coefficients α and β corresponding to different cases:

$$\frac{\sigma_{C_{11}^{\text{eff}}}}{|\nu_{\text{sc}}|} = \alpha \times N_g^{\beta}. \tag{14}$$

In Table 4, the estimated values of coefficients α and β for different cases are summarized. It is worth mentioning that the normalized variabilities of the effective elastic moduli for other components, *e.g.*, C_{12}^{eff} and C_{44}^{eff}, have similar trends as those observed for the component C_{11}^{eff}. However, the values of the parameters α and β are different.

The effect of correlated Euler angles, with varying correlation length parameters, on the normalized standard deviations of effective elastic moduli C_{11}^{eff}, is compared to the uncorrelated case and presented in Figure 7. As expected, the polycrystals with uncorrelated Euler angles have the lowest standard deviation of effective elastic moduli, compared with the polycrystals whose Euler angles are correlated. This could be explained as the uncorrelated Euler angles of the grains in one realization of polycrystal could have more variabilities than the correlated ones. As a result, more variabilities of the Euler angles reduce the statistical anisotropy level of the polycrystal, hence the normalized standard deviation of effective elastic moduli decreases. If the polycrystals are close to theoretical isotropy, then the standard deviations of effective elastic moduli between each realization will tend towards 0.

On the contrary, adding correlations to the Euler angles could reduce their variabilities in each realization and thus increase their anisotropy levels. As such, the standard deviations of effective elastic moduli will have a higher value. This conclusion is shown in Figure 7, where the values of the normalized $\sigma_{C_{11}^{\text{eff}}}$ for the polycrystals whose Euler angles have a longer correlation length (**C-L**) are larger than those having a shorter correlation length (**C-S**). In fact, a relatively long correlation length implies an increase in the characteristic size of heterogeneity. Considering this heterogeneity as an "effective grain" with similar Euler angles and a larger size than the ones in **C-S** and **Uncorrelated** cases, the "effective number of grains" is reduced, leading to increased variability of effective elastic moduli among the realizations of sample sets. Nevertheless, when comparing the **C-S** case with the **Uncorrelated** one, the difference is minimal, particularly for polycrystals with a sufficient number of grains. Therefore, for polycrystals with Euler angles exhibiting relatively short correlation lengths comparable to the grain size, it is acceptable to simulate crystallographic orientations as uncorrelated to simplify the numerical model in order to expedite simulation speed.

In general, our study shows that spatially correlated Euler angles with correlation lengths relatively longer than the grain size can exert a non-negligible impact on the statistical properties of effective elastic moduli in polycrystalline materials. Studying spatially correlated Euler angles of polycrystals holds significant implications for future simulation and experimental studies. By incorporating spatial correlation in simulations, a more realistic representation of polycrystal microstructure is achieved, leading to improved accuracy in predicting macroscopic behavior and mechanical properties. In experimental

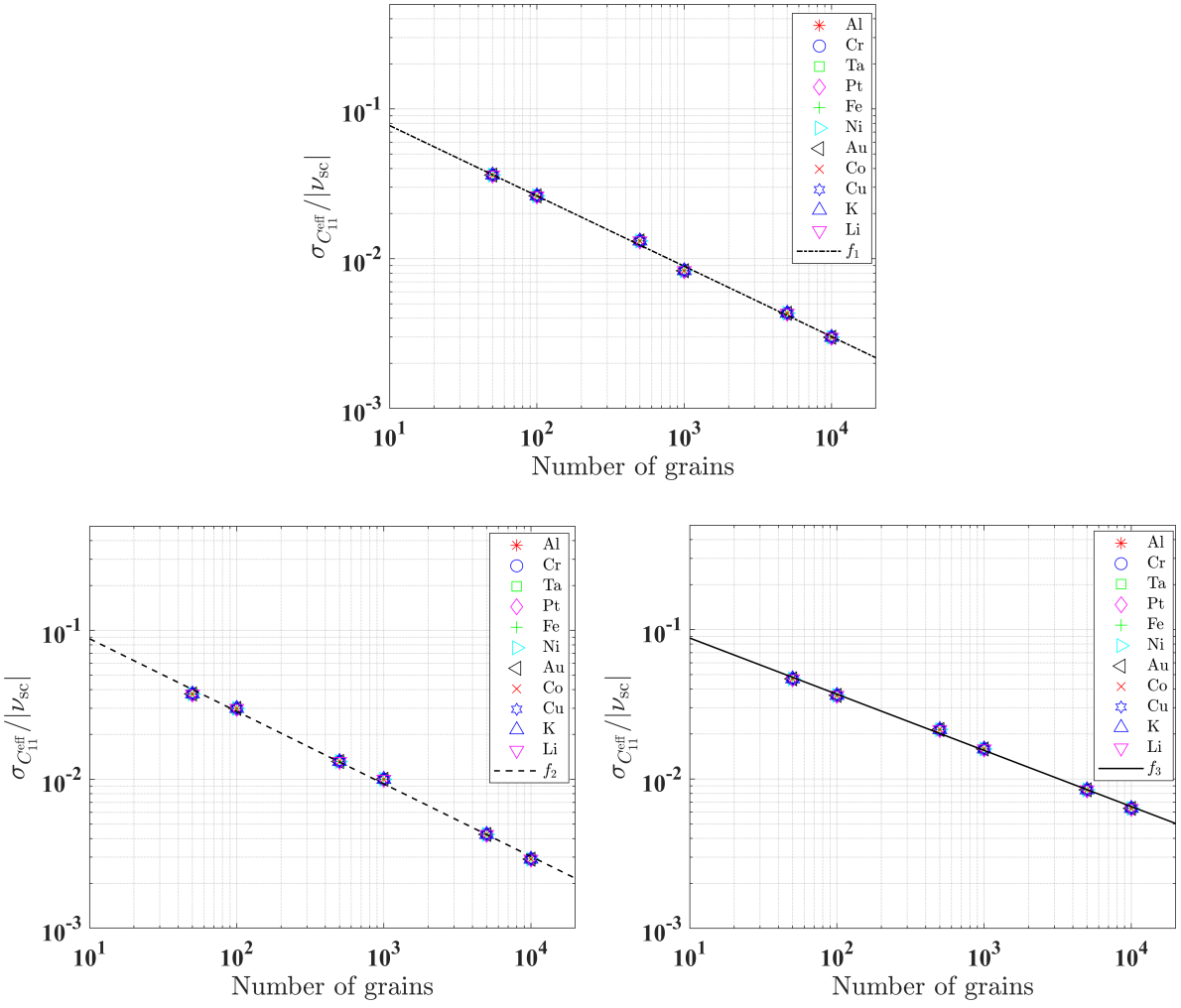

Fig. 6. Normalized standard deviations of C_{11}^{eff}, in terms of the number of grains, for Euler angles with parameters **Uncorrelated** (top), **C-S** (bottom left), and **C-L** (bottom right).

Table 4. Coefficients α and β in equation (14), obtained from numerical results, with three different parameters of Euler angles.

Parameters of Euler angles	α	β
Uncorrelated	0.2287	–0.47
C-S	0.2693	–0.49
C-L	0.2087	–0.38

studies, using the EBSD technique to measure the spatial correlation enables better characterization of polycrystal microstructure, which is crucial for understanding material properties, deformation mechanisms, and failure behaviors. Additionally, including spatial correlation in crystallographic orientations ensures robust predictions, reducing uncertainties in simulations and experimental results. This enhances confidence in the reliability of study outcomes, which is essential for designing and developing materials for critical applications.

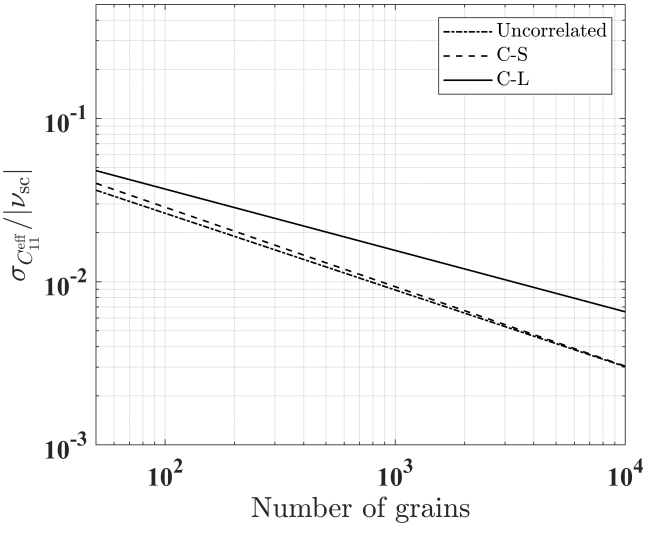

Fig. 7. Main curves of the relation between normalized standard deviations of C_{11}^{eff} and number of grains for Euler angles with **Uncorrelated**, **C-S**, and **C-L** parameters.

4 Conclusion

The influence of the spatially correlated Euler angles on the statistical properties of effective elastic moduli has been investigated in this article based on the synthetic polycrystals of a variety of cubic materials having different anisotropy factors. The random fields of the Euler angles, with an exponential kernel function with two different correlation lengths, are numerically simulated based on the Karhunen–Loève expansion. The effective elasticity tensors of the polycrystals are then estimated by using the classical Eshelby–Kröner Self-Consistent approach. The normalized standard deviations of the effective elastic moduli C_{11}^{eff} are calculated to investigate the statistical properties of the homogenized medium. Results show that apart from the inversely proportional relationship between the normalized standard deviations of C_{11}^{eff} and the number of grains, the spatially correlated Euler angles also influence the statistical properties of effective elastic moduli. The correlation of the Euler angles will increase the standard deviations of the effective elastic properties compared with uncorrelated ones, especially when the correlation lengths exceed the mean grain size. These results highlight the necessity of considering spatially correlated Euler angles in the numerical models based on real polycrystals to enhance the reliability of future numerical investigations. Additionally, the influence of spatially correlated Euler angles on the statistical behaviors of ultrasonic phase velocities as well as the scattering-induced attenuation, is currently under study.

Conflict of Interest

The authors certify that they have no financial conflict of interest in connection with this article.

Funding

This work is financed by Ministère de l'Éducation Nationale de l'Enseignement Supérieur, de la Recherche et de l'Innovation (MESRI). The support of Centre de Calcul Intensif des Pays de la Loire (CCIPL) is gratefully acknowledged.

References

[1] S.I. Ranganathan, M. Ostoja-Starzewski, Scaling function, anisotropy and the size of RVE in elastic random polycrystals, J. Mech. Phys. Solids. **56**, 2773–2791 (2008)

[2] T. Böhlke, K. Jöchen, O. Kraft, D. Löhe, V. Schulze, Elastic properties of polycrystalline microcomponents, Mech. Mater. **42**, 11–23 (2010)

[3] M. Norouzian, J.A. Turner, Ultrasonic wave propagation predictions for polycrystalline materials using three-dimensional synthetic microstructures: Phase velocity variations, J. Acoust. Soc. Am. **145**, 2171–2180 (2019)

[4] S.I. Wright, B.L. Adams, K. Kunze, Application of a new automatic lattice orientation measurement technique to polycrystalline aluminum, Mater. Sci. Eng. A. **160(2)**, 229–240 (1993)

[5] X. Gao, C.P. Przybyla, B.L. Adams, Methodologies for recovering and analyzing two-point pair correlation function in polycrystalline materials, Metall. Mater. Trans. A. **37A**, 2379–2387 (2006)

[6] A. Noshadravan, R. Ghanem, J. Guilleminot, I. Atodaria, P. Peralta, Validation of a probabilistic model for mesoscale elasticity tensor of random polycrystals, Int. J. Uncertain. Quantif. **3** (2013)

[7] R. Quey, P. Dawson, F. Barbe, Large-scale 3D random polycrystals for the finite element method: Generation, meshing and remeshing, Comput. Methods Appl. Mech. Eng. **200**, 1729–1745 (2011)

[8] F. Rhines, B. Patterson, Effect of the degree of prior cold work on the grain volume distribution and the rate of grain growth of recrystallized aluminum, Metall. Mater. Trans. A. **13**, 985–993 (1982)

[9] S. Berbenni, V. Favier, M. Berveiller, Impact of the grain size distribution on the yield stress of heterogeneous materials, Int. J. Plast. **23**, 114–142 (2007)

[10] P.-A. Dubos, E. Hug, S. Thibault, M. Ben Bettaieb, C. Keller, Size effects in thin face-centered cubic metals for different complex forming loadings, Metall. Mater. Trans. A. **44**, 5478–5487 (2013)

[11] M. Ardeljan, R.J. McCabe, I.J. Beyerlein, M. Knezevic, Explicit incorporation of deformation twins into crystal plasticity finite element models, Comput. Methods Appl. Mech. Eng. **295**, 396–413 (2015)

[12] M. Knezevic, B. Drach, M. Ardeljan, I.J. Beyerlein, Three dimensional predictions of grain scale plasticity and grain boundaries using crystal plasticity finite element models, Comput. Methods Appl. Mech. Eng. **277**, 239–259 (2014)

[13] H. Bunge, Texture Analysis in Materials Science: Mathematical Methods. Elsevier, 2013

[14] S. Kullback, R.A. Leibler, On information and sufficiency, Ann. Math. Stat. **22**, 79–86 (1951)

[15] S. Kullback, Information Theory and Statistics, Courier Corporation, 1997

[16] R.G. Ghanem, P.D. Spanos, Stochastic finite element method: Response Statistics, Stochastic Finite Elements: A Spectral Approach, Springer, 1991

[17] M. Loève, Probability Theory. Courier Dover Publications, 2017

[18] S. Khazaie, R. Cottereau, D. Clouteau, Influence of the spatial correlation structure of an elastic random medium on its scattering properties, J. Sound Vib. **370**, 132–148 (2016)

[19] M. Grigoriu, Crossings of non-Gaussian translation processes, J. Eng. Mech. **110**, 610–620 (1984)

[20] M. Grigoriu, Applied Non-Gaussian Processes: Examples, Theory, Simulation, Linear Random Vibration, and MATLAB Solutions, Prentice Hall, Inc., Englewood Cliffs, NJ, 1995

[21] M. Grigoriu, Simulation of stationary non-Gaussian translation processes, J. Eng. Mech. **124**, 121–126 (1998)

[22] J.D. Eshelby, The determination of the elastic field of an ellipsoidal inclusion, and related problems, Proc. Math. Phys. **241**, 376–396 (1957)

[23] E. Kröner, Berechnung der elastischen Konstanten des Vielkristalls aus den Konstanten des Einkristalls, Z. Phys. **151**, 504–518 (1958)

[24] V.A. Lubarda, New estimates of the third-order elastic constants for isotropic aggregates of cubic crystals, J. Mech. Phys. Solids **45**, 471–490 (1997)
[25] C. Zener, Elasticity and Anelasticity of Metals, University of Chicago Press, 1948
[26] A.G. Every, A.K. McCurdy, Second and higher order elastic constants. Landolt–Börnstein Numerical Data and Functional Relationships in Science and Technology New Series Group III: Crystal and Solid State Physics, 1992

Cite this article as: N. Sheng, S. Khazaie, M. Chevreuil, S. Fréour, Statistical properties of effective elastic moduli of random cubic polycrystals, Mechanics & Industry **24**, 33 (2023)